Biochimica et Biophysica Acta 1808 (2011) 2995–3006

Contents lists available at ScienceDirect

Biochimica et Biophysica Acta

journal homepage: www.elsevier.com/locate/bbamem

Thermal, dynamic and structural properties of drug AT_1 antagonist olmesartan in lipid bilayers

Dimitrios Ntountaniotis [a,b], Gregor Mali [c,e], Simona Golic Grdadolnik [d,e], Halabalaki Maria [f], Alexios-Leandros Skaltsounis [f], Constantinos Potamitis [b], Eleni Siapi [b], Petros Chatzigeorgiou [g], Michael Rappolt [h,*], Thomas Mavromoustakos [i,**]

[a] Department of Chemistry, University of Patras, Patras 26500, Greece
[b] National Hellenic Research Foundation, Institute of Organic and Pharmaceutical Chemistry, 48 Vas. Constantinou, 11635, Athens, Greece
[c] Laboratory for Inorganic Chemistry and Technology, National Institute of Chemistry, Hajdrihova 19, SI-1001 Ljubljana, Slovenia
[d] Laboratory of Biomolecular Structure, National Institute of Chemistry, Hajdrihova 19, SI-1001 Ljubljana, Slovenia
[e] EN-FIST Centre of Excellence, Dunajska 156, SI-1000 Ljubljana, Slovenia
[f] University of Athens, Department of Pharmacy, Pharmacognosy Section, Zographou 15771, Athens, Greece
[g] University of Athens, Department of Chemistry, Laboratory of Physical Chemistry, Zographou 15771, Athens, Greece
[h] Austrian Academy of Sciences, Institute of Biophysics and Nanosystems Research (IBN), c/o Sincrotrone Trieste, Strada Statale 14, km 163.5, 34149 Basovizza, Italy
[i] University of Athens, Department of Chemistry, Laboratory of Organic Chemistry, Zographou 15771, Athens, Greece

ARTICLE INFO

Article history:
Received 26 May 2011
Received in revised form 14 July 2011
Accepted 1 August 2011
Available online 6 August 2011

Keywords:
Olmesartan
Dipalmitoyl-phosphatidylcholine bilayer
Small-angle and wide angle X-ray scattering
Raman spectroscopy
Differential scanning calorimetry
Solid state NMR spectroscopy

ABSTRACT

It is proposed that AT_1 antagonists (ARBs) exert their biological action by inserting into the lipid membrane and then diffuse to the active site of AT_1 receptor. Thus, lipid bilayers are expected to be actively involved and play a critical role in drug action. For this reason, the thermal, dynamic and structural effects of olmesartan alone and together with cholesterol were studied using differential scanning calorimetry (DSC), ^{13}C magic-angle spinning (MAS) nuclear magnetic resonance (NMR), cross-polarization (CP) MAS NMR, and Raman spectroscopy as well as small- and wide angle X-ray scattering (SAXS and WAXS) on dipalmitoyl-phosphatidylcholine (DPPC) multilamellar vesicles. ^{13}C CP/MAS spectra provided direct evidence for the incorporation of olmesartan and cholesterol in lipid bilayers. Raman and X-ray data revealed how both molecules modify the bilayer's properties. Olmesartan locates itself at the head-group region and upper segment of the lipid bilayers as ^{13}C CP/MAS spectra show that its presence causes significant chemical shift changes mainly in the A ring of the steroidal part of cholesterol. The influence of olmesartan on DPPC/cholesterol bilayers is less pronounced. Although, olmesartan and cholesterol are residing at the same region of the lipid bilayers, due to their different sizes, display distinct impacts on the bilayer's properties. Cholesterol broadens significantly the main transition, abolishes the pre-transition, and decreases the membrane fluidity above the main transition. Olmesartan is the only so far studied ARB that increases the *gauche*:*trans* ratio in the liquid crystalline phase. These significant differences of olmesartan may in part explain its distinct pharmacological profile.

1. Introduction

Hypertension is a chronic medical condition, which affects approximately one billion people worldwide [1,2]. The renin–angiotensin aldosterone system (RAAS) modulates blood pressure and it is the major system associated with hypertension. Many classes of antihypertensive medication are developed to act on RAAS. Angiotensin II receptor blockers (ARBs) have been designed to inhibit the binding of angiotensin II (AII) onto the G-protein coupled AT_1 receptor, and consequently decrease blood pressure [3–6]. Apart from complications such as stroke, ischemic heart disease, vascular remodeling and diabetic nephropathy, AII is associated also with inflammation, oxidative stress and cell growth [1,7–9]. Olmesartan medoxomil (Fig. 1A) belongs to the antihypertensive class of ARBs. This drug is an ester prodrug of the active metabolite (Fig. 1B), which is deesterified in the gastrointestinal tract [10,11]. The IUPAC name of this active metabolite olmesartan is 5-(2-hydroxypropan-2-yl)-2-propyl-3-[[4-[2-(2H-tetrazol-5-yl) phenyl] phenyl] methyl] imidazole-4-carboxylic acid.

Olmesartan medoxomil is commonly prescribed with a thiazide diuretic (in general, hydrochlorothiazide (HCT)) and/or a calcium channel blocker to ameliorate its effect [12–14]. The Food and Drug Administration (FDA) approved olmesartan medoxomil on April

* Corresponding author. Tel.: +39 040 375 8708; fax: +39 040 375 8029.
**Corresponding author. Tel.: +30 2107274475; fax: +30 2107274761.
E-mail addresses: michael.rappolt@elettra.trieste.it (M. Rappolt), tmavrom@chem.uoa.gr (T. Mavromoustakos).

0005-2736/$ – see front matter © 2011 Elsevier B.V. All rights reserved.
doi:10.1016/j.bbamem.2011.08.001

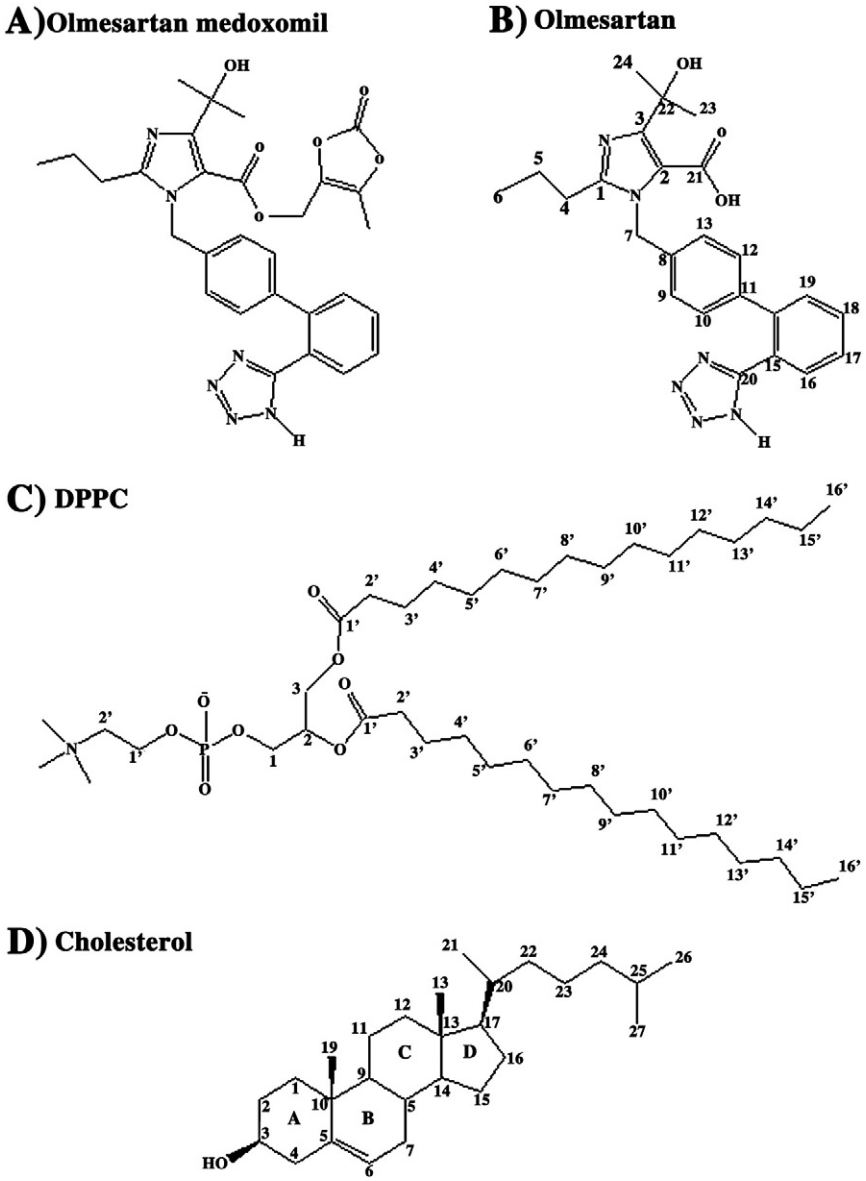

Fig. 1. The chemical structures of (A) prodrug olmesartan medoxomil; (B) olmesartan; (C) DPPC; and D) cholesterol.

2002, which was the seventh drug in the class of ARBs [15]. It has been marketed as an antihypertensive drug in United States, Japan and European countries [16]. The most recent approval by FDA was announced on July 2010 for Tribenzor (olmesartan medoxomil, amlodipine, hydrochlorothiazide), a new three-in-one combination product for the treatment of hypertension, which contains an ARB, a calcium channel blocker and a diuretic [17]. Although olmesartan belongs to ARB class, it is proposed that its pharmacological profile is distinct from the others. Generally, not only pharmacological similarities but also differences are observed among different ARBs [11,18].

In this study, liquid and solid state nuclear magnetic resonance (NMR), differential scanning calorimetry (DSC), Raman spectroscopy as well as small- and wide angle X-ray scattering (SAXS, WAXS) were applied to investigate the thermal, dynamic and structural properties of olmesartan in dipalmitoyl-phosphatidylcholine (DPPC) bilayers in the absence and presence of cholesterol.

In our previous studies we have put forward a two-step model in which the AT_1 prototype antagonist losartan first inserts into the bilayer core and diffuses towards the active site (first step), and then anchors to the active site (second step) [19]. As a continuation of our studies we are now examining and comparing the effects of AT_1 antagonist olmesartan with losartan and other AT_1 antagonists in liposomal formulations to reveal their role in distribution and eventually try to explain their drug efficacies.

In this work, multilamellar vesicles (MLVs) of dipalmitoyl-phosphatidylcholine (DPPC) (Fig. 1C) formed in excess of water were used to model the plasma membranes of vasculature. Note, that saturated phosphatidylcholines are the most abundant lipid species in the plasma membrane of vasculature (40–65%) [20].

In the past DPPC MLVs have been extensively used in NMR and DSC experiments to study the interactions of lipid-soluble drugs with biological membranes as the main phase transitions occur at convenient temperatures and are close to physiological ones [21–26]. Cholesterol (Fig. 1D) is a major component of the cell plasma membrane and its role is essential to establish proper membrane permeability and fluidity as well as to interfere with drug action [27–29].

The aim of this research work is to study olmesartan–lipid interactions in a temperature range from 20 °C up to 50 °C covering all mesomorphic phases. DSC experiments using samples with different molar ratios (olmesartan:phospholipid) were prepared.

Further, to understand the influence of cholesterol, DPPC:cholesterol bilayers were formulated by adding different concentrations of the drug. The idea behind the use of cholesterol is to simulate closer the membrane lipidic environment.

The expected insight into the studied biomimetic systems is manifold due to the given set of complementary methods applied. Briefly, DSC provides valuable information on the thermal modifications that are caused by the presence of drugs in the membrane [26]. Performed solid state NMR experiments included ^{13}C magic angle spinning (MAS) and ^{13}C cross polarization/magic angle spinning spectroscopy (CP/MAS). These techniques offer useful information for the dynamic changes that drugs cause when they are incorporated in the lipid bilayers [30–33]. Typical observations are related with chemical shift or intensity changes of various key atoms which are partitioning in the membrane. Chemical shift changes are further associated with phase transition properties of the membrane bilayer. Moreover new peaks arise because of the presence of the drug [27]. Raman and X-ray diffraction experiments provide complementary structural information, for instance regarding interdigitation effects of the molecules in lipid bilayers [34]. All together, these techniques characterize the properties of olmesartan especially in comparison with other AT_1 antagonists which were studied in our laboratory. On these grounds, also the distinct pharmacological similarities and differences of olmesartan to other ARBs are highlighted.

2. Materials and methods

2.1. Materials

Olmesartan was kindly donated from Daiichi Sankyo Pro Pharma, Japan. Dipalmitoyl-phosphatidylcholine was purchased from Avanti Polar Lipids Inc. (Alabaster, AL). Cholesterol and methanol were purchased from Sigma Aldrich (St. Louis, MO).

2.2. Methods

2.2.1. Differential scanning calorimetry

To prepare the samples for DSC experiments, appropriate amounts of DPPC, olmesartan and cholesterol, diluted in chloroform/methanol were mixed, dried under stream of argon and then stored under high vacuum overnight. Distilled and deionized water was added to the dried mixtures of DPPC–olmesartan and DPPC–cholesterol–olmesartan to produce a 50% (w/w) mixture/water preparation (or water/lipid molar ratio ranging from 41 to 52 depending on the mixture). The samples were transferred to stainless steel capsules obtained from Perkin-Elmer and sealed. Thermal scans were obtained on a Perkin-Elmer DSC-7 instrument (Norwalk, CT). All samples were scanned from 10 to 60 °C at least three times until identical thermal scans were obtained using a scanning rate of 2.5 °C/min. The temperature scale of the calorimeter was calibrated using indium ($T_m = 156.6$ °C) and DPPC bilayers ($T_m = 41.2$ °C). The following diagnostic parameters were used for the study of drug to membrane interactions: T_m (maximum position of the recorded heat capacity), T_{onset} (the starting temperature of the phase transition) and $\Delta T_{m1/2}$ (the full width at half maximum of the phase transition), and the respective parameters concerning the pre-transition. An empty pan for the base line and a sample containing double distilled water were run for the temperature range of 10–60 °C as a reference for the background. This background was subtracted from each thermal scan of the samples. The area under the peak, represents the enthalpy change during the transition (ΔH). The mean values of ΔH of three identical scans were tabulated.

The drug concentrations used for the different experiments were $x = 0.05$ (5 mol% olmesartan) and $x = 0.20$ (20 mol% olmesartan). For ternary mixtures, a fixed DPPC/cholesterol ratio was kept (15 mol% cholesterol), and either 5 mol% olmesartan or 20 mol% olmesartan were added.

2.2.2. Solid state NMR

The procedure to prepare the samples for ^{13}C MAS and ^{13}C CP/MAS spectroscopy was identical to that applied for DSC samples. Briefly, distilled and deionized water was added to the dried binary mixtures of DPPC/olmesartan and ternary mixtures of DPPC/cholesterol/olmesartan to produce a 50% (w/w) liposome dispersion. The samples were transferred to 3.2 mm zirconia rotors. ^{13}C NMR spectra were obtained at 150.80 MHz with a 600 MHz Varian spectrometer (Palo Alto, CA). The spinning rate used was 5 kHz. The experimental temperatures were 25 °C, 35 °C, and 45 °C for ^{13}C CP/MAS experiments and 45 °C for the ^{13}C MAS measurement.

2.2.3. High resolution liquid NMR

The high-resolution NMR spectra were recorded on a Varian DirectDrive 800 MHz spectrometer at 25 °C. Spectra were obtained with 2 mg of sample dissolved in 0.7 ml CD_3OD (Sigma Aldrich, St. Louis, MO). Default parameters installed in the library of the spectrometer were used. The ^1H and ^{13}C chemical shift assignments were obtained in a standard way using DQF-COSY, TOCSY, NOESY, HSQC, and HMBC 2D experiments. Spectra were collected in the phase sensitive mode using the pulse sequences in the Varian library of pulse programs. Spectra allowed the unambiguous assignment of olmesartan.

2.2.4. Raman spectroscopy

Raman spectra were recorded with a Perkin-Elmer GX Fourier Transform spectrometer (Shelton, CT). A diode pumped Nd:YAG laser at 1064 nm (Norwalk, CT) was used as the excitation source. The scattered radiation was collected at an angle of 180° with respect to the incident beam. Spectra were recorded at a laser power of 400 mW on sample with a resolution of 2 cm^{-1}. To obtain a good signal-to-noise ratio, 2500 scans were coadded for each spectrum. The temperature was controlled using the high-temperature cell (CAL 3300, Ventacon Ltd, Winchester, UK). The intensity of a Raman band was observed over a period of 15 min. Analysis of the spectra was carried out using the Spectrum Software Version No. 3.02.01 (Perkin-Elmer, Norwalk, CT). Raman spectra of the examined samples were obtained in the frequency region of 3500–400 cm^{-1} and in the temperature range 25 to 50 °C.

2.2.5. X-ray scattering experiments

Time resolved simultaneous small- and wide-angle X-ray scattering (SAXS and WAXS) experiments were carried out at the Austrian SAXS beamline at ELETTRA, Trieste [35,36]. The 1D position sensitive detector [37] for SAXS covered the s-range ($s = 2\sin(\theta)/\lambda$ with 2θ being the scattering angle and $\lambda = 1.54$ Å the applied X-ray wavelength) of interest from about 1/250 $Å^{-1}$ to 1/12 $Å^{-1}$. The WAXS detector (same type) covered the s-range from 1/9.4 to 1/3.2 $Å^{-1}$. The angular calibration was performed with silver-behenate ($CH_3(CH_2)_{20}$–COOAg: d-spacing 58.38 Å [38]) for the SAXS regime, and for the WAXS regime the diffraction pattern of p-bromobenzoic acid was used as reference [39]. The lipid dispersion was measured in a thin-walled 1 mm diameter quartz capillary in a steel cuvette (Anton Paar, Graz, Austria), which was inserted into a brass block. This sample holder block was in thermal contact with a water circuit, i.e. it was connected to a water bath with a freely programmable control unit (Unistat CC, Huber, Offenburg, Germany). In order to avoid air convection at the capillary, the entrance and exit windows of the block have been covered with a thin polymer film. The temperature was measured in the vicinity of the capillary in the sample holder block with a Pt-element (100 Ω). Prior to the temperature scan, the sample was equilibrated for a period of 10 min at 20 °C. Static control experiments before and after the scans were taken with an exposure time of 120 s. For the time resolved experiments the samples were heated from 20 to 60 °C and back to 20 °C with a scan rate of 1 °C/min taking every minute exposures with a duration of 15 s. During the

waiting periods of 45 s a small solenoid driven shutter was closed in order to keep the radiation dosage in the samples as small as possible.

2.2.5.1. X-ray data-analysis. In the time resolved X-ray scattering experiments the first order diffraction peaks of the different gel and liquid crystalline phases (reflections with the highest intensity) were used to derive the lattice spacings in the SAXS and WAXS regime, respectively, by standard procedures as described in ref. [40,41]. Briefly, after the raw data had been corrected for detector efficiency and the background scattering both from water and the sample cell had been subtracted, all Bragg peaks were fitted by Lorentzian distributions, and the diffuse WAXS contribution arising from the fluid chain packing with a Gaussian distribution. The fittings were carried out with home written procedures running under IDL 5.2 (Research Systems, Inc., USA). Few static scattering patterns were analyzed by fitting the form factor contributions with a simple bilayer model [42,43]. This model uses one Gaussian for the head-groups and another for the hydrophobic core.

3. Results

3.1. Differential scanning calorimetry

The progressive thermal effects of olmesartan in DPPC bilayers are shown in Fig. 2. The major thermal changes of olmesartan are observed on the pre-transition. Already at a low concentration of 5 mol%, olmesartan broadens and lowers the pre-transition temperature (see Table 1). At a drug concentration of 20 mol% the pre-transition is almost invisible, and also concerning the main transition $\Delta T_{m1/2}$ is broadened and T_m lowered, although not very significantly (Table 1, Fig. 2). ΔH is not affected either at low or at high drug concentrations (see also SF1).

The thermal effects of olmesartan on DPPC/cholesterol bilayers (85:15 molar ratio) is shown in Fig. 2. At 15 mol% cholesterol is well known to abolish the pre-transition of DPPC bilayers, and cholesterol somewhat broadens the main phase transition and slightly decreases T_m[44]. Moreover, it causes a significant lowering of ΔH (Table 1). In this case, the addition of olmesartan (5 mol%) appears to not modify significantly the thermal events. Thus, it does not cause any significant changes in T_m, $\Delta T_{m1/2}$ and ΔH (SF1).

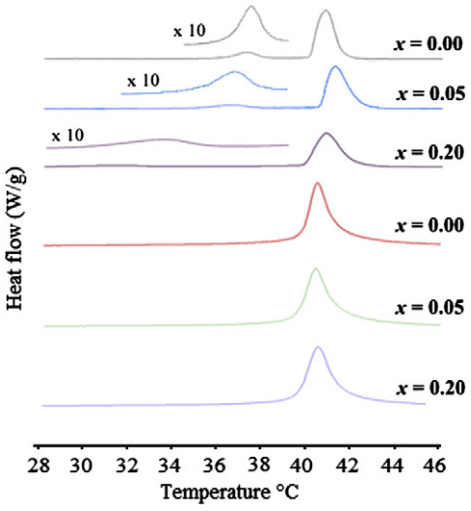

Fig. 2. DSC thermal scans for samples with different lipid/drug/sterol molar ratios. From top to the bottom: DPPC 100%, DPPC/olmesartan (95:5), DPPC/olmesartan (80:20), DPPC/cholesterol (85:15) [DPPC/cholesterol]/olmesartan (95:5), and [DPPC/cholesterol]/olmesartan (80:20). The DPPC:cholesterol ratio for the two last samples is 85:15.

Table 1
Diagnostic parameters ΔH, T_{onset}, T_m and $\Delta T_{m1/2}$ of the DSC experiments.

DPPC/olmesartan						
	0 mol% olmesartan		5 mol% olmesartan		20 mol% olmesartan	
	Pre-trans.	Main trans.	Pre-trans.	Main trans.	Pre-trans.	Main trans.
ΔH (J/g)	6.3	41.8	5.5	43.0	3.2	42.7
T_m (°C)	37.6	41.2	37.0	41.6	31.9	41.2
$\Delta T_{m1/2}$	1.0	0.9	1.8	1.0	2.9	1.3

DPPC/cholesterol/olmesartan (cholesterol fixed at 15 mol%)			
	0 mol% olmesartan	5 mol% olmesartan	20 mol% olmesartan
	Main trans.	Main trans.	Main trans.
ΔH (J/g)	29.2	29.2	31.0
T_m (°C)	40.6	40.5	40.6
$\Delta T_{m1/2}$	1.0	1.1	1.2

3.2. ^{13}C MAS and CP/MAS NMR spectroscopy

To obtain detailed local information on the incorporation of olmesartan and cholesterol in the DPPC bilayers, we applied high-resolution NMR spectroscopy using magic angle spinning without or with cross polarization [45].

The thermal effects of olmesartan in DPPC bilayers alone or with cholesterol or olmesartan or the mixture of cholesterol/olmesartan are shown in Fig. 3 (see also SF2–SF5). Each spectrum was divided into three regions, namely concerning the carbon atoms in the (i) hydrophobic region (10–40 ppm), those in the (ii) glycerol and backbone region (40–80 ppm) and in the (iii) esterified carbonyls (near 170 ppm).

3.2.1. Hydrophobic region

The chemical shift decreases (upfield effect), when DPPC bilayers undergo the transition from the lamellar gel phase $L_{\beta'}$ (25 °C) towards the ripple phase $P_{\beta'}$ (35 °C) and lamellar liquid crystalline phase L_α (45 °C) (Table 2). This is due to the strong *trans:gauche* isomerisation effects observed especially in the turnover to the L_α phase. For example, we detected an upfield change between 0.2 and 2.2 ppm for $(CH_2)'_{10}$, C-14′, C-15′ and C-16′ signifying the same trend and different extent of upfield effect of the carbons that constitute the hydrophobic region. Upfield effect (0.2–1.8 ppm) was also observed in DPPC/cholesterol and DPPC/olmesartan bilayer (0.2–2.1 ppm) samples [46,47].

3.2.2. Head-group region

Smaller changes were observed for the four preparations used in our experiments indicating that head-group conformational changes from gel to liquid crystalline phase are less pronounced compared to that observed in the hydrophobic region (Table 2). The effect of cholesterol or olmesartan has been examined in the head-group region by comparing the chemical shifts of the lipid bilayers in the absence and presence of cholesterol or olmesartan at identical temperatures. Chemical shifts of DPPC/olmesartan were almost identical with those of DPPC/cholesterol preparation. Thus, olmesartan exerts the same effect as cholesterol in this head-group region. In addition, the effect of cholesterol or olmesartan was less pronounced than that observed in the hydrophobic region. To study the combined effect of cholesterol and olmesartan, the preparation DPPC/cholesterol/olmesartan has been compared with those of DPPC/cholesterol and DPPC/olmesartan. The chemical shifts of all three preparations are almost identical, indicating that combined effect of olmesartan with cholesterol is identical to those of cholesterol or olmesartan alone.

3.2.3. Glycerol backbone region

A downfield shift (<0.11 ppm) was observed during the phase transition from the gel to liquid crystalline state indicating its

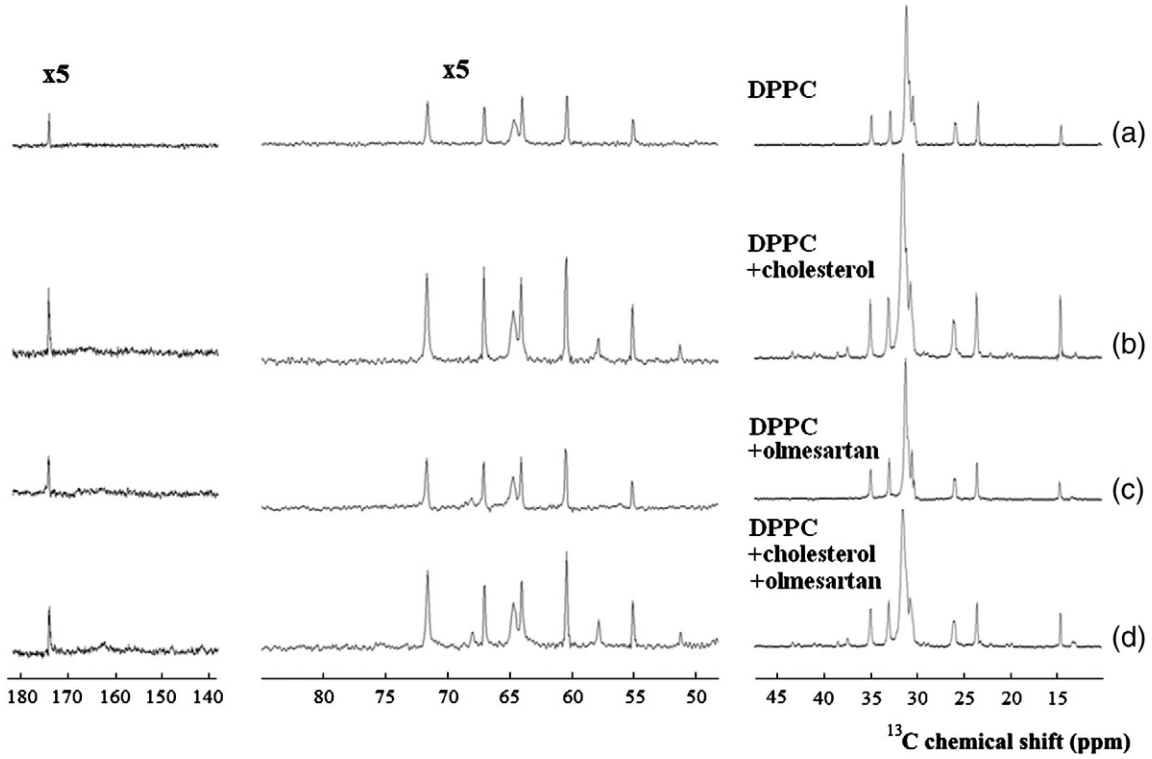

Fig. 3. ^{13}C CP/MAS spectra at 45 °C for DPPC; DPPC/cholesterol (85:15); DPPC/olmesartan (80:20); and [DPPC/cholesterol]/olmesartan (80:20).

conformational stability in this bilayer region for the preparations DPPC, DPPC/cholesterol, DPPC/olmesartan. For the DPPC/cholesterol/olmesartan sample a downfield effect was already eminent in the ripple phase (>0.2 ppm) (Table 2).

3.2.4. Carbonyl region

The resolution for C-1′ in the four preparations was not sufficient to follow the chemical shift changes during the phase transition (Table 2). In DPPC bilayers for C-2′, a biphasic effect was observed, i.e. a downfield effect in the ripple phase and an upfield effect in the liquid crystalline phase. For C-3′ a progressive upfield effect was eminent as the temperature increases reaching approximately 1 ppm in the L_α phase, indicating that this carbon in the carbonyl region behaves similarly to all other carbons belonging to the hydrophobic region. Similar effects were observed for the DPPC/cholesterol sample. For DPPC/olmesartan bilayers an upfield effect was observed for carbonyl groups, which means an opposite trend in comparison to the DPPC and DPPC/cholesterol samples. For C-3′ a progressive upfield effect was observed, and for C-2′, a biphasic effect was seen like in the DPPC and DPPC/cholesterol samples. When both olmesartan and cholesterol are incorporated in DPPC bilayers, a small downfield effect was observed for carbonyl groups and a small upfield effect was

Table 2
Observed chemical shifts for DPPC carbons in ^{13}C MAS and ^{13}C CP/MAS experiments.

T (°C)	Sample	C-X												
		C-1	C-2	C-3	C-1′, C-1″	C-2′, C-2″	C-3′, C-3″	$(CH_2)'_{10}$, $(CH_2)''_{10}$	C-14′, C-14″	C-15′, C-15″	C-16′, C16″	$N(CH_3)_3$	C-2‴	C-1‴
^{13}C MAS														
45	DPPC	63.80	71.41	64.41	174.02	34.81	25.86	31.10	32.83	23.41	14.49	54.89	66.82	60.21
	DPPC/cholesterol	63.88	71.45	64.53	174.19 +174.00	34.93	26.04	31.51	33.00	23.54	14.55	54.93	66.84	60.28
	DPPC/olmesartan	63.85	71.44	64.48	174.13	34.89	25.94	31.18	32.92	23.51	14.62	54.93	66.86	60.28
	(DPPC/cholesterol)/olmesartan	63.87	71.45	64.51	174.10 +173.92	34.89	25.90	31.48	32.96	23.50	14.50	54.92	66.85	60.27
^{13}C CP/MAS														
25	DPPC	–	71.22	64.38	172–175	34.98	26.72	33.25	34.22	24.45	14.65	54.76	66.63	60.22
	DPPC/cholesterol	–	71.22	64.48	172–175	35.15	26.82	33.26	34.26	24.48	14.70	54.79	66.66	60.26
	DPPC/olmesartan	–	71.28	64.46	172–175	35.11	26.82	33.31	34.31	24.55	14.77	54.82	66.67	60.28
	(DPPC/cholesterol)/olmesartan	63.74	71.21	64.49	172–175	35.15	26.90	33.37	–	24.55	14.69	54.83	66.69	60.29
35	DPPC	–	71.14	64.38	172–175	35.10	26.37	33.11	–	24.25	14.60	54.79	66.69	60.20
	DPPC/cholesterol	–	71.21	64.47	172–175	35.19	26.46	33.10	–	24.29	14.65	54.92	66.81	60.33
	DPPC/olmesartan	–	71.40	64.56	172–175	35.19	26.41	33.19	–	24.30	14.67	54.91	66.83	60.33
	(DPPC/cholesterol)/olmesartan	–	71.48	64.50	174.52	34.18	25.46	32.99	–	24.29	14.66	54.90	66.80	60.32
45	DPPC	63.77	71.37	64.49	174.03	34.81	25.85	31.06	32.79	23.39	14.49	54.86	66.81	60.19
	DPPC/cholesterol	63.86	71.43	64.55	174.17	34.93	26.02	31.43	32.97	23.53	14.55	54.93	66.85	60.27
	DPPC/olmesartan	63.84	71.43	64.57	174.13	34.89	25.94	31.16	32.91	23.51	14.60	54.93	66.87	60.27
	(DPPC/cholesterol)/olmesartan	63.89	71.45	64.56	174.16	34.90	26.01	31.43	32.94	23.52	14.56	54.94	66.87	60.28

produced for C-2′ and C-3′. The effect of cholesterol in this region was probed by comparing the DPPC and DPPC/cholesterol samples. Small downfield changes attributed to cholesterol were also observed in all mesomorphic states for C-2′ and C-3′. DPPC/olmesartan chemical shifts are almost identical to those of DPPC/cholesterol, suggesting that olmesartan and cholesterol cause the same effect in this region. An exception was observed in the ripple phase where the DPPC/olmesartan sample showed an upfield effect on DPPC bilayers, while DPPC/cholesterol displayed a downfield effect.

3.3. Raman spectroscopy

Raman spectra of pure DPPC bilayers and in the presence of 20 mol% olmesartan alone or with 10 mol% cholesterol were obtained in a temperature range of 26–50 °C. The spectra were recorded in a range of 400–3500 cm^{-1} (Fig. 4). The transition behavior was especially characterized by the C–C and C–H stretching modes. In particular, the C–H stretching bands at ~2850 cm^{-1} and ~2880 cm^{-1} have been analyzed, which are assigned to symmetric and antisymmetric stretching modes in the methylene groups (CH_2) of the alkyl chains, respectively, while the band at ~2935 cm^{-1} is correlated to the chain terminal methyl C–H symmetric stretching mode [48,49]. Further, spectral bands in the spectral region 1000–1200 cm^{-1} related to the C–C stretching modes have been investigated [50]. The bands at ~1090 cm^{-1} and ~1130 cm^{-1} reflect the C–C stretching modes in *gauche* and *trans* conformations, respectively. (For a recent overview on Raman spectra of DPPC bilayers see ref. [51]).

3.4. X-ray scattering

In Fig. 5, an overview of all carried out time-resolved SAXS/WAXS experiments is given. In the contour plots high scattering intensities are color-coded with red and orange, while lower scattering intensities are given in green and blue. In Fig. 5A the widely studied phase behavior of DPPC bilayers [52], and the corresponding structural changes are illustrated. Here, we shall repeat only briefly the phase sequence. From 20 to about 36 °C the lamellar gel phase ($L_{\beta'}$) is existent [53]. The chains are tilted with respect to the bilayer plane with about 32° [54], and are packed in an orthogonal lattice [55,56]. Thereafter, the stable ripple phase ($P_{\beta'}$) gets induced at about 36 °C [57,58]. Due to additional freedom in chain rotation, the hydrocarbon chains pack here on a hexagonal lattice. At about 42 °C the chains melt and the lamellar liquid crystalline phase is observed (L_α) [59]. Note, that the transition is not reversible, but in cooling direction two ripple phases form: the stable and the so-called metastable ripple phase ($P_{\beta'}$ and $P_{\beta'\ mtstbl}$). The later phase has a ripple repeat distance that is about two times as big as that of the stable ripple phase [58,60]. Second, the $L_{\beta'}$ phase is not readily formed in cooling direction, but instead a lamellar phase with a pronounced stacking disorder can be seen. Also the interaction of cholesterol with phosphatidylcholine bilayers has been widely studied [27,44,61,62], and the main thermodynamic events are shown in Fig. 5B. At 10 mol% cholesterol content a part of the phospholipids change their original conformation, i.e. cholesterol induces the so called liquid ordered phase (lo). This phase coexists with both, the gel-phase and also with the L_α phase. Since the lipids in the lo-state are free to diffuse laterally, the membrane below T_m becomes more fluid, but on the other hand, since the lipids in the lo-state display an *all-trans* chain conformation the *gauche*:*trans* ratio decreases above T_m.

Strikingly, as can be seen in the SAXS patterns of Fig. 5C, olmesartan provokes in the gel phase regime the unbinding of bilayer membranes: it does not form multilamellar, but unilamellar vesicles (see also Fig. 6, bottom curve). The unbinding is most probably caused by electrostatic repulsion (membrane undulation usually plays a minor role in the gel phase). In the liquid crystalline phase instead, multilamellar vesicles are again apparent. In contrast to the effect of olmesartan alone (Fig. 5C), the incorporation of olmesartan together with cholesterol in the DPPC bilayers induces again multilamellar vesicles also in the gel phase (Fig. 5D). In fact the phase behavior of DPPC/olmesartan/cholesterol bilayers is very alike to DPPC/cholesterol system. This is obvious when comparing panel B with panel D.

The temperature dependent lamellar repeat distance, *d*, and lipid chain packing of the four studied samples is presented in Fig. 7. The *d*-

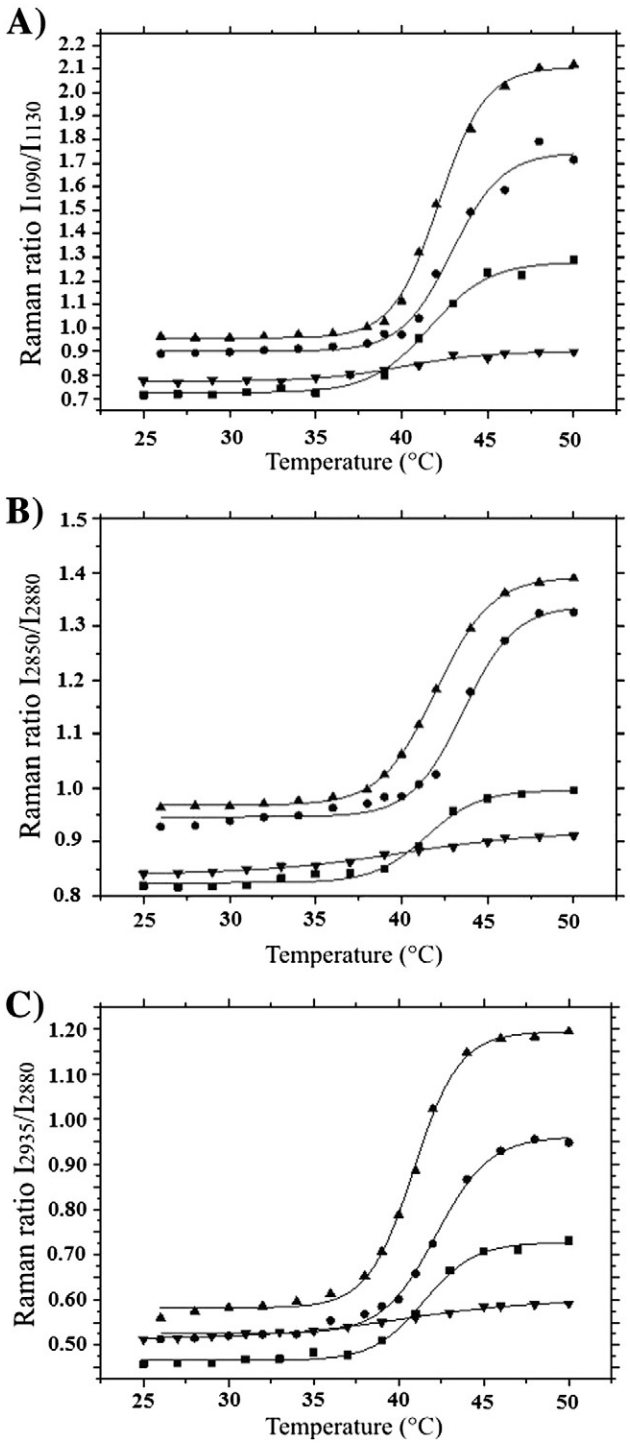

Fig. 4. (A) I1090/I1130 vs. temperature plots for pure DPPC (squares), DPPC containing x = 0.20 of olmesartan (circles), DPPC/olmesartan with x = 0.10 cholesterol (triangles up), and DPPC containing x = 0.10 cholesterol alone (triangles down). With the same symbolic meaning as in panel A the (B) I2850/I2880 vs. temperature plots and (C) I2935/I2880 vs. temperature are depicted.

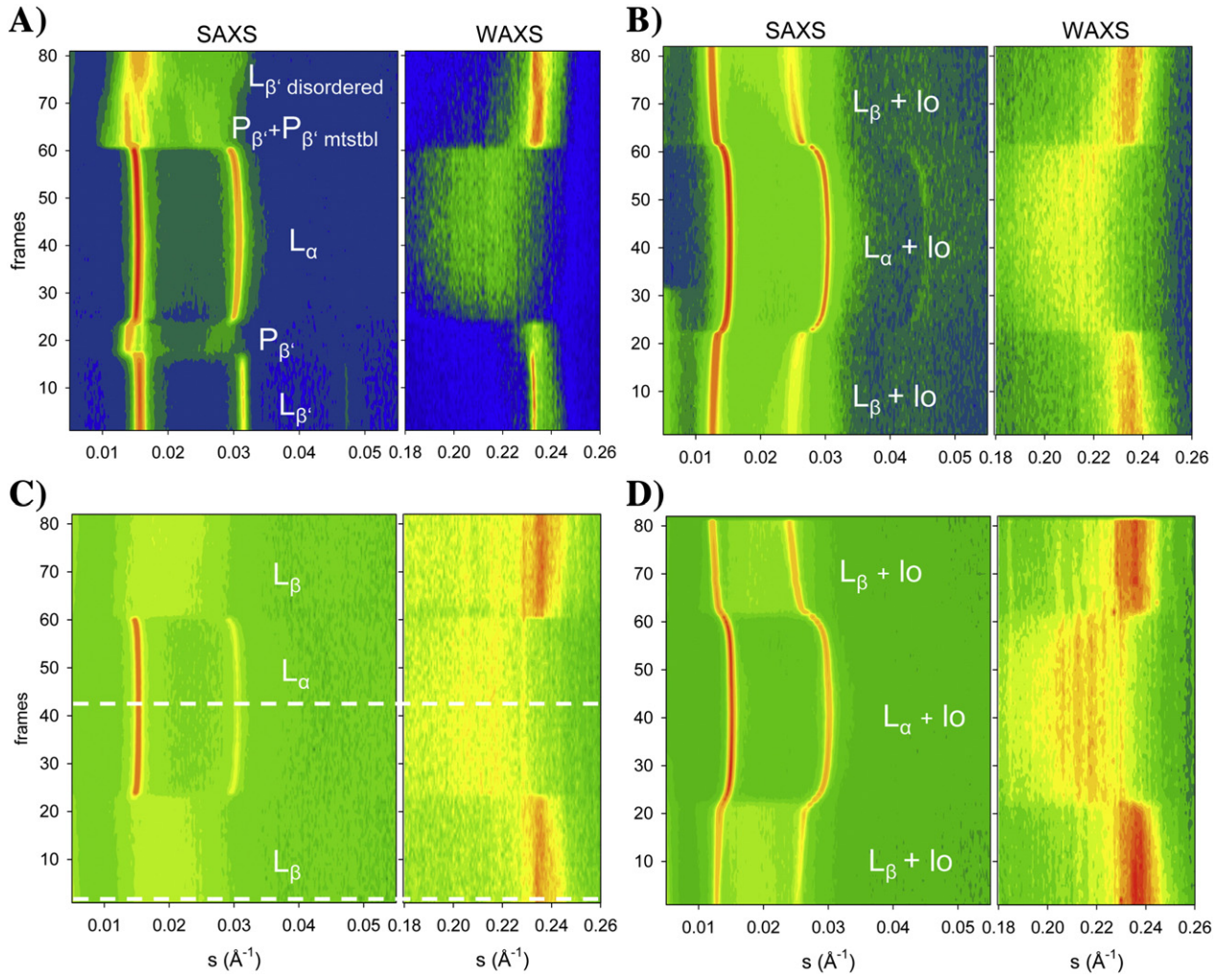

Fig. 5. Temperature scan of multilamellar vesicles basing on DPPC from 20 to 60 °C and back to 20 °C with 1 °C/min. Note, frame numbers 1 and 80 refer to 20 °C, and the maximum temperature was reached at frame 40. (A) Pure DPPC vesicles under excess of water conditions, (B) multilamellar vesicles of DPPC/cholesterol (90/10 molar ratio), (C) vesicles containing DPPC/olmesartan (80/20), and (D) vesicles composed of DPPC/cholesterol/olmesartan (70/10/20) were investigated. Horizontal dashed lines in panel C refer to extracted X-ray scattering patterns shown in Fig. 6.

spacing trends of the membrane stacking in the liquid crystalline phase are similar, i.e. the anomalous swelling behavior [63,64] in the vicinity of the melting point are alike (Fig. 7A). The absolute *d*-values

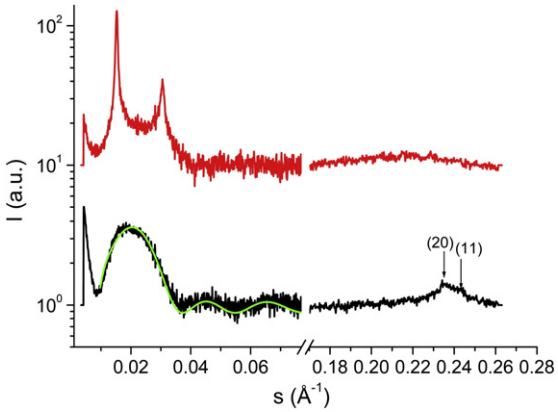

Fig. 6. SAXS and WAXS patterns of vesicles containing DPPC/olmesartan (80/20 mol/mol) at 20 (black line) and 60 °C (red line), respectively. The patterns refer to the temperature scan depicted in Fig. 5C. The form factor scattering in gel-phase has been fitted applying a simple bilayer model (solid green line).

though differ a bit: the biggest membrane repeat is found for ternary lipid bilayers (66.6 Å at 50 °C), followed by DPPC/cholesterol (66.2 Å), DPPC/olmesartan (65.8 Å), and finally completed by pure DPPC bilayers (65.2 Å). The lipid chain packing gives a relative good indication for the main transition temperature, T_m (Figs. 7B–D). The melting point for DPPC alone and DPPC/olmesartan is determined with the WAXS recordings to be at 42.5 °C, while for DPPC/cholesterol and DPPC/olmesartan/cholesterol T_m is about 1 degree lower, i.e. $T_m = 41.5$ °C. Please note, that the absolute transition temperature for the loss of long range order in the chain packing is about 1 °C higher as expected from observed the chain melting transition temperature obtained from the DSC measurements (cp. Table 1). This small retardation in the structural rearrangements of chain packing is probably due to the chosen scan rate of 1 °C/min. At scan rates of 0.1 °C/min and less, the thermal and structural events should superimpose, see e.g. reference [65].

4. Discussion

4.1. Differential scanning calorimetry

The thermal behavior of olmesartan in lipid bilayers shows that mainly the head-group region is affected. This conclusion is drawn, because actually only the pre-transition gets abolished, i.e. the ripple

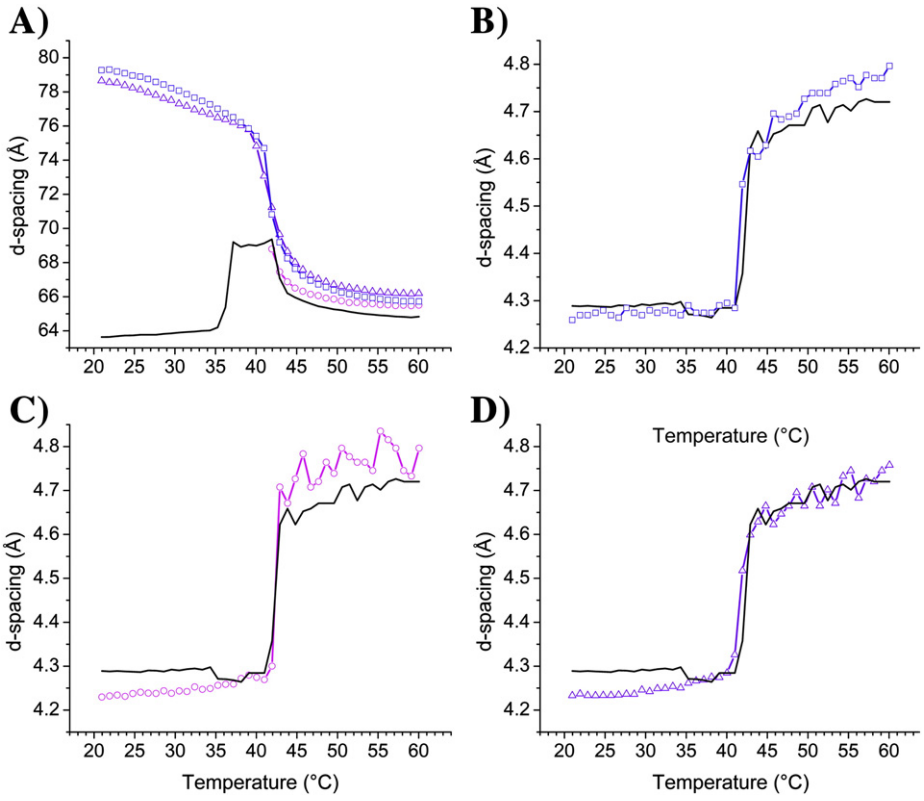

Fig. 7. (A) Lamellar repeat distance, d, as function of temperature for DPPC (black), DPPC/cholesterol (blue), DPPC/olmesartan (magenta), and DPPC/olmesartan/cholesterol bilayers. (B, C, D) The nearest neighbor chain to chain distances derived from the first order diffraction peaks in the gel phase, and rough distances determined from the position of the diffuse scattering maximum in the liquid crystalline phase are displayed. Samples are the same as in Fig. 5.

phase gets suppressed at high olmesartan content indicating that the mismatch of projected head-group to lipid chain area gets reduced. On the other hand, losartan has no significant effect on the main phase transition; definitely olmesartan does not increase ΔH. This is in contrast to valsartan and losartan, were an increase in the main transition enthalpy was accounted mainly to an increase in volume expansion work during the main transition [19,66]. Thus, it appears that olmesartan probably interacts on the head-group region and upper segment of the alkyl chains, but less strongly with the hydrophobic core of the bilayer as losartan and valsartan that have been shown to induce at least partial chain interdigitation. Candesartan, although showing similar thermal profiles with olmesartan, does increase ΔH significantly [67]. The fact that olmesartan did not impose any ΔH increase, indicates that it induces no lipid interdigitation [33,68]. This is also confirmed by the X-ray data as discussed below.

The similarities and differences of olmesartan with other ARBs can be interpreted as follows: both olmesartan and candesartan are disturbing less the chain packing in the lipid bilayers, since they have no extensive alkyl chains. Such an observation is in agreement with reported results published recently by Makriyannis et al. [69] using deuterium solid state NMR spectroscopy. However, such behavior cannot be accounted just by examining their lipophilic profile [70].

The thermal behavior of olmesartan in DPPC/cholesterol bilayers provides less evidence that the drug molecule exerts its action on the head-group. Since cholesterol by itself abolishes the pre-transition any additional effect attributed to the drug olmesartan is obscured. Even the presence of olmesartan at 20% does not cause any significant change in the main transition temperature and its width (Table 1). However, it increases ΔH, although this increase is still lower than that observed with DPPC bilayers alone (SF1).

4.2. ^{13}C MAS and CP/MAS NMR spectroscopy

^{13}C CP/MAS spectra showed that the effect of cholesterol or olmesartan was less pronounced in the head-group in comparison to that exerted in the hydrophobic region. This is in agreement with the Raman spectroscopy data as both cholesterol and olmesartan affected significantly the *gauche:trans* ratio. The downfield effect exerted by both cholesterol and olmesartan at glycerol backbone and carbonyl regions indicate that both molecules affect this region.

^{13}C NMR spectroscopy allows comparing the dynamic effects of olmesartan with cholesterol and other ARBs. The results attributed to cholesterol or olmesartan are summarized (see ST1 and ST2). Due to the low intensity of the olmesartan peaks, they are not evidently visible in Fig. 3 and SF2–SF4. In terms of peaks attributed to cholesterol, the following observation can be made: almost all peaks attributed to the four rings and alkyl chains are eminent and grow in intensity as the temperature increases. This shows that cholesterol is embedded in the membrane with considerable motion. The most prominent chemical shift changes relatively to those observed in solid cholesterol are those referring to the A-ring (see Fig. 1D). This indicates that the cholesterol A-ring is in spatial vicinity of the polar part of the lipid bilayers (i.e. C1 differs 1.2–1.3 ppm from the reference).

In contrast to cholesterol, only few olmesartan peaks were observed, reflecting the rigidity of the molecule in lipid bilayers. The peaks attributed to the aromatic rings are characterized as broad and of low in intensity. Interestingly, this is observed both, in ^{13}C CP/MAS and ^{13}C MAS experiments indicating that the small intensity and broad peaks observed are not due to the insufficient cross polarization. The fact that in the ^{13}C MAS experiments the peaks are barely seen, is attributed to the low sensitivity of this experiment as compared to the cross

polarization experiments. Flexibility was observed only on the alkyl chain of olmesartan. The above observations show that olmesartan has different dynamic properties in the lipid bilayers than cholesterol. Two plausible explanations can be given: (a) the aromatic part of olmesartan is more rigidified in the bilayer core when compared to cholesterol and/or (b) a smaller amount of drug is incorporated in the lipid bilayers. This second explanation is in accordance with DSC data which show no additional thermal effect of the drug and X-ray results which give a hint for a reduced drug-membrane affinity in the gel phase when DPPC/cholesterol bilayers are applied.

In comparison to our previous studies [19] using solid state ^{13}C MAS for DPPC/losartan preparation some distinct differences can be realized. Losartan aromatic peaks were prominent, easily to be identified and sharper. Thus, it appears that biphenyltetrazole ring of the two AT_1 antagonists shows distinct mobility. Losartan's biphenyltetrazole is more mobile than that of olmesartan. This explains the differential thermal properties of olmesartan and losartan. Losartan anchors with tetrazole ring in the head-group region (note, that this drug is provided as a salt and has negative charge on the tetrazole), while the alkyl chain is more flexible in the lipidic core. This topographical position in lipid bilayers is reflected as abolishment of the pre-transition temperature and lowering of the main phase transition already at low losartan concentrations. Olmesartan does not have such a strong anchoring, although clearly is situated in the vicinity of the head-group. This is reflected in the fact that the pre-transition does not get completely abolished and it rather increases the main phase transition temperature. Nevertheless, it fits and packs properly in lipid bilayers.

The significance of the aromatic packing was shown also in our previous work. We showed that membranes restrict the motion of a pair of inactive–active pair of steroids Δ^{16}-alphaxalone–alphaxalone respectively in a different manner [71]. Interestingly, we have also shown that the inactive analog was not incorporated in high degree in membranes in contrast to the fully incorporation of the active analog [72]. We have also shown that the aromatic part of the inactive analog Me-Δ^8-THC was more mobile than its active psychomimetic analog Δ^8-THC [32,33]. These results show that solid-state NMR is capable of differentiating between the effects of structurally very similar compounds. Such observation is in agreement with the conclusions by Santos et al. who observed different effects in the case of structurally related tricyclic antidepressants desipramine and imipramine [73].

4.3. Raman spectroscopy

Intramolecular *trans–gauche* conformational changes within the hydrocarbon chain region can be monitored directly by the intensity ratio I_{1090}/I_{1130}. This peak height intensity ratio allows the direct comparison of the bilayers order–disorder transitions between liposome preparations without or with drug incorporation [74]. In Fig. 4A the changes in I_{1090}/I_{1130} intensity ratio in pure DPPC, DPPC/cholesterol as well as DPPC/olmesartan and DPPC/olmesartan/cholesterol bilayers are presented. The transition temperatures compare well to the results found from the calorimetric measurements and are clearly indicated. DPPC shows a strong ΔI increase across the gel to liquid crystalline phase ($\Delta I = 1.29–0.71 = 0.58$, which means an increase of 81.2%). This increase is smaller with cholesterol indicating especially its condensing effect in the liquid crystalline phase (0.78 to 0.90 or 15.5%). On the other hand, olmesartan induces an increase of the *gauche-trans* ratio across the gel to liquid crystalline phase transition: ΔI increases from 0.89 to about 1.71 ($\Delta I = 0.83$), which means an increase of about 93%. Cholesterol together with olmesartan causes a further increase during the main phase ($\Delta I = 2.12–0.96 = 1.1$ (115.7%)). These results signify that both olmesartan and olmesartan/cholesterol mixture increase entropy changes during the main phase transition.

Interestingly, the presence of losartan, valsartan or candesartan lower the ΔI values [66,75] which is opposite to the effect of olmesartan. Thus, in DPPC bilayers the chain mobility changes decrease by the formerly studied three AT_1 antagonists, while it increases for olmesartan.

The most intense bands in the Raman spectrum of lipid samples are given in the methylene C–H stretching mode region 2800–3000 cm^{-1}, which are commonly used to monitor changes in the lateral packing properties and mobility of the lipid chain in both gel and liquid crystalline bilayer systems [76]. In particular, the analysis of the symmetrical and antisymmetrical methylene stretching bands allows investigating the thermotropic phase behavior of lipids. Levin and co-workers were the first to introduce the intensity ratio of these two bands I_{2850}/I_{2880} as an order parameter [77]. This ratio describes the main change occurring in the hydrocarbon-chain region of the lipids and corresponds to intermolecular interactions among aliphatic chains. It is sensitive to subtle changes in conformational order from rotations, kinks, twists and bends of the lipid chains [78]. Alike to the ratio I_{1090}/I_{1130} the presence of olmesartan or olmesartan/cholesterol causes significant increase also in the I_{2850}/I_{2880} meaning that both, drug alone or in the present of cholesterol cause disorder in the lipid bilayers (Fig. 4B). The same applies for the ratio I_{2935}/I_{2880} (Fig. 4C). Thus, consistently the three ratios show that olmesartan causes fluidization of the lipid bilayers which is strengthened by the incorporation of cholesterol.

Other characteristic band alterations in the liquid crystalline phase provide evidence for the incorporation of olmesartan in the monolayer leaflets of the DPPC membrane. First, the band at 715 cm^{-1} which corresponds to C–N symmetric stretching vibration of the polar head-group [79] of DPPC bilayers shows a downshifting of 1 cm^{-1} in the examined temperature range, when olmesartan is incorporated in lipid bilayers (data not shown). This is the opposite effect to that observed for candesartan [74], losartan [19,34,80] and valsartan [75], but similar to the effects observed for dipeptide and non-steroidal anti-inflammatory molecules [81,82] which bind only loosely to the head-group area. Last, the presence of olmesartan in DPPC/cholesterol bilayers causes an upshifting of the 715 cm^{-1} band and the temperature profile of this band behaves like DPPC bilayers alone. These results show that cholesterol and olmesartan have an opposite effect on head–group interactions.

Second, the band at 1294 cm^{-1} which corresponds to $(CH)_2$ twisting vibration of the acyl chains [83] of DPPC bilayers shows an upshifting of 1 cm^{-1} in the examined temperature range, when olmesartan is present in DPPC bilayers. Cholesterol has a synergistic effect, since it shifted this band to even higher wavenumbers (data not shown). These results are in accordance with the three ratios (Fig. 4), that confirm an increase of the lipid bilayer's fluidity with the presence of olmesartan, which is even enhanced when cholesterol is added.

Third, a new peak at 1024 cm^{-1} which corresponds to the "breathing" of the aromatic rings of olmesartan clearly identifies the incorporation of it in DPPC bilayers (data not shown) in accordance with solid state NMR data (see ST2) [84].

4.4. X-ray scattering

The integration of olmesartan to pure DPPC bilayers causes in the gel-phase the unbinding of membranes (Fig. 5C). As mentioned above, this is understood to be due to the electrostatic repulsion, which is caused by the membrane surface charges in the presence of olmesartan. Olmesartan has a rather low pK_a value of 4.3 [85], and therefore a high ratio of ionized form is likely to show up at pH 7. Please note, that a similar unbinding behavior has been observed also for losartan loaded PC-vesicles (data not shown), which has an even lower pK_a value of 3.15 [86]. Nevertheless, increasing the temperature and passing the melting point, the membranes rebind again, i.e.

multilamellar vesicles are formed (Fig. 6). This probably means that the electrostatic repulsion decreases above T_m. A possible explanation lies in the increase of the area per molecule (about 30%), which in turn would lead to a decrease in the surface charge density, and hence to a reduction in the electrostatic repulsion, if the olmesartan concentration in the bilayers remains the same. Remarkably, as we could show recently [75], also the DPPC/valsartan bilayers exhibit a reduction of the overall repulsion force above T_m, although the effect was not as strong. This is plausible though, given the higher pK_a value of 4.9 for valsartan [86]. Nevertheless, other effects like a different penetration depths of olmesartan in the fluid bilayer and/or a diminished olmesartan partitioning in the fluid bilayers could also decrease the electrostatic repulsion force. However, the transition is reversible (Fig. 5C), which makes a strong expulsion of olmesartan from the fluid bilayers less probable. Nevertheless, further analysis of the scattering curve at 20 °C (Fig. 6, bottom curve) reveals that olmesartan has no big influence onto the chain region of the DPPC bilayers, i.e. there is no measurable effect on the bilayer thickness. We find that the head-group to head-group distance, d_{HH}, is 44.6 ± 0.4 Å, which compares very well with the published value of 44.2 Å for pure DPPC bilayers [59]. This is in contrast to other ARBs, which are able to induce at least partial interdigitation in the gel-phase, which has for instance recently been demonstrated for the action of valsartan on DPPC vesicles [75]. As can be seen in the WAXS regime (Fig. 6, bottom right), also the chain-packing remains unaltered: the underlying orthorhombic lattice displays the typical sharp (20)-reflection (arrow) with a d_{20}-spacing of 4.27 Å together with the broader (11)-reflection (arrow) with a d_{11}-spacing of about 4.17 Å. This compares well to the pure DPPC data from Sun et al. [56], who published the values $d_{20} = 4.244$ Å and $d_{11} = 4.182$ Å for pure DPPC vesicles at 24 °C.

Completely different is the situation, when olmesartan is added to DPPC/cholesterol bilayers (Fig. 5D). Here olmesartan does not induce any unbinding of membranes. An explanation could be that the affinity of olmesartan for the DPPC/cholesterol bilayers is reduced as compared to pure DPPC bilayers. This actually would also mean that the electrostatic repulsion gets reduced in the ternary bilayer system. Further, when comparing the overall lattice spacings (d-values) of the DPPC/olmesartan/cholesterol and DPPC/cholesterol systems (Fig. 7A), no big difference is seen over the whole temperature range. This actually also supports the interpretation, that the affinity of the DPPC/cholesterol bilayers are not in favor for the olmesartan up-take.

The temperature dependent analysis of the chain packing (Figs. 7B–D) does not reveal any further surprises. In agreement with the DSC data in the DPPC/cholesterol samples (Figs. 7B and D) the chain melting transition temperature is reduced about 1 °C, while the addition of olmesartan alone (Fig. 7C) does not change the T_m (compare also DSC data, Table 1). This is readily understood, since cholesterol in low concentrations can be considered as impurity in the DPPC bilayers, and hence a lowering of the melting point is expected.

5. Conclusion

^{13}C CP/MAS spectra provided direct evidence for the incorporation of cholesterol and olmesartan in lipid bilayers as many peaks in the spectra can be attributed to their presence. DSC, Raman spectroscopy and X-ray diffraction data are in accordance with the NMR data, since the presence of the cholesterol or olmesartan does modifies some of the observed key parameters of the lipid bilayers. X-ray diffraction data demonstrate in addition that under neutral pH conditions a high fraction of olmesartan molecules are ionized (bilayer unbinding in the gel-phase), and further we observed that the affinity of olmesartan for DPPC/cholesterol bilayers is reduced as compared to pure DPPC bilayers. This might have important biological consequences in the drug diffusion towards the active site of the receptor as it is well known that cholesterol is one of the major constituent of lipid bilayers.

Olmesartan is most probably located at the head-group region and upper segment of the membranes, because it does not affect significantly the chemical shifts of alkyl chain segment of cholesterol in the DPPC/cholesterol/olmesartan bilayers. Thus, the effect of olmesartan is restrained on the head-group, glycerol and carbonyl region and upper segment of the alkyl chain region of the lipid membranes.

Additional evidence that olmesartan mainly effects the head-group region is given by the DSC results. Although olmesartan and cholesterol are competing or residing at the same topographical membrane region, due to their different sizes and flexibility exert different effects. While olmesartan affects significantly only the pre-transition, cholesterol not only abolishes the pre-transition, but also exerts also significant effects in the main transition (lowering its cooperativity and decreasing the T_m).

Of great interest though is the fact that olmesartan shows distinct dynamic properties in lipid bilayers which differ from other ARBs so far studied. For example, in our previous work [75] we showed that valsartan caused a decrease in the bilayer thickness due to partial lipid interdigitation. Such an effect was not observed with olmesartan as X-ray diffraction data confirmed a constant bilayer in the gel-phase. Further, no indication for an olmesartan induced phase separation is given as supported also by the DSC and Raman spectroscopy data.

In addition, valsartan and losartan cause differential modifications in the thermal changes of lipid bilayers [67,75]. Valsartan and losartan abolish the pre-transition already at low concentrations and cause a significant lowering of the main phase transition temperature. Olmesartan, on the other hand, only at high concentrations afforded the abolishment of the pre-transition and has no significant effect on the main phase transition temperature. Candesartan, losartan and valsartan cause an increase in ΔH and of the *trans*:*gauche* ratio [67,68,75], but although olmesartan causes a strong decrease in the *trans*:*gauche* ratio, it does not affect ΔH significantly. All these differences propose a different mode of action of olmesartan when it is incorporated in the lipid bilayers.

The emerging picture is that although all ARBs so far studied appear to localize in the head-group regime, they affect differently both the head-group and the alkyl chain region. Olmesartan causes the least structural changes on the polar/apolar membrane interface attributed probably due to smaller penetration depths in bilayers and concurring aggregations in the water phase [87]. These associations are, however, expected to be less effective in the liquid crystalline matrix of the membranes, since at sufficient concentrations the drug succeeds to embed also in the upper hydrophobic core. Such limitation in the effectiveness is not seen with losartan and valsartan. Candesartan CV shows similar property with olmesartan in this respect [67].

From this analysis it appears that each ARB molecule appears to have its own fingerprint regarding thermal and dynamic interactions with lipid bilayers, even if all of them reside at the bilayer–water interface. This explains their common site of action (i.e. AT_1 receptor), but gives also a hint for their different pharmacological properties. The different properties of ARBs provide an important message. Lipid/ARB interactions might be the selective key, which in the end determine the unique pharmacological response. However, more studies starting from simple and then leading to more complex biomimetic model systems are necessary to pin down the individual functionalities of differently designed membrane active drugs.

Acknowledgments

T. Mavromoustakos acknowledges the receipt of time working at European synchrotron facilities in Trieste. T. Mavromoustakos and D. Ntountaniotis acknowledge EENC program for covering the travel and residence expenses to perform NMR experiments in the Slovenian

NMR Centre. The NMR studies were supported by EN-FIST Centre of Excellence (Dunajska 156, SI-1000 Ljubljana, Slovenia) and Slovenian Research Agency.

Appendix A. Supplementary data

Supplementary data to this article can be found online at doi:10.1016/j.bbamem.2011.08.001.

References

[1] A.M. Bell, D. Nykamp, Hypertension: focus on olmesartan medoxomil clinical medicine, Therapeutics 1 (2009) 1–9.
[2] A. Ferro, R. Gilbert, H. Krum, Importance of renin in blood pressure regulation and therapeutic potential of renin inhibition, Int. J. Clin. Pract. 60 (5) (2006) 577–581.
[3] K.S. Babu, A.R. Tagore, G.S. Reddy, G. Venkateswarlu, P.P. Reddy, R.V. Anand, Synthesis of related substances of olmesartan medoxomil, anti-hypertensive drug, Arkivoc II (2010) 292–302.
[4] C. Potamitis, M. Zervou, V. Katsiaras, P. Zoumpoulakis, S. Durdagi, M.G. Papadopoulos, J.M. Hayes, S.G. Grdadolnik, I. Kyrikou, D. Argyropoulos, G. Vatougia, T. Mavromoustakos, Antihypertensive drug valsartan in solution and at the AT_1 receptor: conformational analysis, dynamic NMR spectroscopy, *in silico* docking and molecular dynamics simulations, J. Chem. Inf. Model. 49 (2009) 726–739.
[5] M. Burnier, Angiotensin II type 1 receptor blockers, Circulation 103 (2001) 904–912.
[6] M. de Gasparo, K.J. Catt, T. Inagami, J.W. Wright, T. Unger, International union of pharmacology. XXIII. The angiotensin II receptors, Pharmacol. Rev. 52 (3) (2000) 415–472.
[7] R.M. Touyz, Intracellular mechanisms involved in vascular remodeling of resistance arteries in hypertension: role of angiotensin II, Exp. Physiol. 90 (2005) 449–455.
[8] H. Kobori, N. Masaomi, G. Navar, A. Nishiyama, The intrarenal renin–angiotensin system: from physiology to the pathobiology of hypertension and kidney disease, Pharmacol. Rev. 59 (3) (2007) 251–287.
[9] Y. Kyotani, J. Zhao, S. Tomita, H. Nakayama, M. Isosaki, M. Uno, M. Yoshizumi, Olmesartan inhibits angiotensin II-induced migration of vascular smooth muscle cells through Src and mitogen-activated protein kinase pathways, J. Pharmacol. Sci. 113 (2010) 161–168.
[10] T. Murakami, H. Konno, N. Fukutsu, M. Onodera, T. Kawasaki, F. Kusu, Identification of a degradation product in stressed tablets of olmesartan medoxomil by the complementary use of HPLC hyphenated techniques, J. Pharm. Biomed. Anal. 47 (2008) 553–559.
[11] D.E. Mire, T.N. Silfani, M.K. Pugsley, A review of the structural and functional features of olmesartam medoxomil, an angiotensin receptor blocker, J. Cardiovasc. Pharmacol. 46 (5) (2005) 585–593.
[12] M.A.M. Gomes, A.D. de Magalhães Feitosa, W. Oigman, J.M. Ribeiro, E.H. Moriguchi, J.F.K. Saraiva, D.B. Précoma, A.B. Ribeiro, C. Amodeo, A.A. Brandão, Based treatment algorithm for essenssial hypertension with olmesartan medoxomil, Arq. Bras. Cardiol. 91 (3) (2008) 168–176.
[13] L.M. Ruilope, Clinical efficacy and safety of olmesartan/hydrochlorothiazide combination therapy in patients with essential hypertension, Vasc. Health Risk Manag. 4 (6) (2008) 1237–1248.
[14] M. Greathouse, Olmesartan medoxomil combined with hydrochlorothiazide for the treatment of hypertension, Vasc. Health Risk Manag. 2 (4) (2006) 401–409.
[15] D. Norwood, E. Branch, B. Smith, M. Honeywell, Olmesartan medoxomil for hypertension: a clinical review, Pharm. Ther. 27 (2002) 611–618.
[16] P. Mehulkumar, V. Ramesh, V. Vinay kumar, R. Srinivas, V. Diwan Prakash, Simultaneous spectroscopic estimation of amlodipine besylate and olmesartan medoximil in tablet dosage form, Asian J. Res. Chem. 2 (2) (2009) 127–130.
[17] Daiichi Sankyo, Inc. TRIBENZOR Prescribing Information.
[18] M.A. Adams, L. Trudeau, Irbesartan: review of pharmacology and comparative properties, Can. J. Clin. Pharmacol. 7 (1) (2000) 22–31.
[19] P. Zoumpoulakis, I. Daliani, M. Zervou, I. Kyrikou, E. Siapi, G. Lamprinidis, E. Mikros, T. Mavromoustakos, Losartan's molecular basis of interaction with membranes and AT_1 receptor, Chem. Phys. Lipids 125 (1) (2003) 13–25.
[20] M. Paul, A.P. Mehr, R. Kreutz, Physiology of local renin–angiotensin systems, Physiol. Rev. 86 (2006) 747–803.
[21] L. Zhao, S.S. Feng, N. Kocherginsky, I. Kostetski, DSC and EPR investigations on effects of cholesterol component on molecular interactions between paclitaxel and phospholipid within lipid bilayer membrane, Int. J. Pharm. 338 (2007) 258–266.
[22] S. Fujisawa, M. Ishihara, Y. Kadoma, pH-dependent complexation of methacryloyloxydecyl dihydrogen phosphate (MDP) with dipalmitoyl-phosphatidylcholine (DPPC) liposomes: DSC and NMR measurements, Internet Electron. J. Mol. Des. 5 (2006) 49–59.
[23] K. Wójtowicz, Comparison of the effect of 4-hydroxycoumarin and umbelliferone on the phase transition of dipalmitoylphosphatidylcholine (DPPC) bilayers, Pharmacol. Rep. 60 (2008) 555–560.
[24] F. Castelli, C. Messina, M.G. Sarpietro, R. Pignatello, G. Puglisi, Flurbiprofen release from Eudragit RS and RL aqueous nanosuspensions: a kinetic study by DSC and dialysis experiments, AAPS PharmSciTech 3 (2) (2002) (article 9).
[25] M.C. Sainz, J.R. Chantres, B. Elorza, M.A. Elorza, DSC study of the action of phenylbutazone on DMPC and DPPC bilayers, Int. J. Pharm. 89 (3) (1993) 183–190.
[26] T. Mavromoustakos, The use of differential scanning calorimetry to study drug–membrane interactions, in: Alex M. Dopico (Ed.), Methods Molecular Biology, 400, Humana Press, 2007, pp. 587–600.
[27] A. Hodzic, M. Rappolt, H. Amenitsch, P. Laggner, G. Pabst, Differential modulation of membrane structure and fluctuations by plant sterols and cholesterol, Biophys. J. 94 (2008) 3935–3944.
[28] J. Pan, T.T. Mills, S. Tristram-Nagle, J.F. Nagle, Cholesterol perturbs lipid bilayers nonuniversally, Phys. Rev. Lett. 100 (19) (2008) 198103.
[29] A. Ramamoorthy, D.K. Lee, T. Narasimhaswamy, R.P.R. Nanga, Cholesterol reduces pardaxin's dynamics—a barrel-stave mechanism of membrane disruption investigated by solid-state NMR, Biochim. Biophys. Acta 1798 (2010) 223–227.
[30] U. Holzgrabe, I. Wawer, B. Diehl, NMR Spectroscopy in Pharmaceutical Analysis, First ed. Elsevier, 2008.
[31] C. Song, H. Holmsen, W. Nerdal, Existence of lipid microdomains in bilayer of dipalmitoylphosphatidylcholine (DPPC) and 1-stearoyl-2-docosahexenoyl-phosphatidyl-serine (SDPS) and their perturbation by chlorpromazine: a ^{13}C and ^{31}P solid-state NMR study, Biophys. Chem. 120 (2006) 178–187.
[32] T. Mavromoustakos, I. Daliani, Effects of cannabinoids in membrane bilayers containing cholesterol, Biochim. Biophys. Acta 1420 (1999) 252–265.
[33] T. Mavromoustakos, E. Theodoropoulou, A combined use of ^{13}C-cross polarization: magic angle spinning, ^{13}C-magic angle spinning and ^{31}P-nuclear magnetic resonance spectroscopy with differential scanning calorimetry to study cannabinoid–membrane interactions, Chem. Phys. Lipids 92 (1998) 37–52.
[34] T. Mavromoustakos, P. Chatzigeorgiou, C. Koukoulitsa, S. Durdagi, Partial interdigitation of lipid bilayers, Int. J. Quantum Chem. 6 (2011) 1172–1183.
[35] H. Amenitsch, M. Rappolt, M. Kriechbaum, H. Mio, P. Laggner, S. Bernstorff, First performance assessment of the small-angle X-ray scattering beamline at ELETTRA, J. Synchrotron Radiat. 5 (1998) 506–508.
[36] S. Bernstorff, H. Amenitsch, P. Laggner, High-throughput asymmetric double-crystal monochromator of the SAXS beamline at ELETTRA, J. Synchrotron Radiat. 5 (1998) 1215–1221.
[37] A.M. Petrascu, M.H.J. Koch, A. Gabriel, A beginners' guide to gas-filled proportional detectors with delay line readout, J. Macromol. Sci. B 37 (1998) 463–483.
[38] T.C. Huang, H. Toraya, T.N. Blanton, Y. Wu, X-ray powder diffraction analysis of silver behenate, a possible low-angle diffraction standard, J. Appl. Crystallogr. 26 (1993) 180–184.
[39] K. Ohkura, S. Kashino, M. Haisa, Crystal structure of p-bromobenzoic acid, Bull. Chem. Soc. Jpn. 45 (1972) 2651–2653.
[40] M. Rappolt, A. Hodzic, B. Sartori, M. Ollivon, P. Laggner, Conformational and hydrational properties during the Lbeta to Lalpha and Lalpha to HII-phase transition in phosphatidylethanolamine, Chem. Phys. Lipids 154 (2008) 46–55.
[41] M. Rappolt, The biologically relevant lipid mesophases as "seen" by X-rays, in: A. Leitmannova-Liu (Ed.), Advances in Planar Lipid Bilayers and Liposomes, vol. 5, Elsevier Inc., Amsterdam, 2006, pp. 253–283.
[42] G. Pabst, M. Rappolt, H. Amenitsch, P. Laggner, Structural information from multilamellar liposomes at full hydration: full q-range fitting with high-quality X-ray data, Phys. Rev. E 62 (2000) 4000–4009.
[43] M. Rappolt, Bilayer thickness estimations with "poor" diffraction data, J. Appl. Phys. 107 (084701) (2010) 1–7.
[44] M.R. Vist, J.H. Davis, Phase equilibria of cholesterol/dimpalmitoyl–phosphatidylcholine mixtures: ^2H nuclear magnetic resonance and differential scanning calorimetry, Biochemistry 29 (1990) 451–464.
[45] A. Ramamoorthy, Beyond NMR spectra of antimicrobial peptides: dynamical images at atomic resolution and functional insights, Solid State Nucl. Magn. Reson. 35 (2009) 201–207.
[46] W. Guo, J.A. Hamilton, A multinuclear solid-state NMR study of phospholipid–cholesterol interactions. Dipalmitoylphosphatidylcholine–cholesterol binary system, Biochemistry 34 (1995) 14174–14184.
[47] C. López, R.M. Claramunt, J. Elguero, Oxalic acid/phenols and oxalic acid/cholesterol co-crystals: a solid state ^{13}C CPMAS NMR study, Arkivoc IV (2008) 33–46.
[48] R.C. Spiker, I.W. Levin, Raman spectra and vibrational assignments for dipalmitoylphosphatidylcholine and structurally related molecules, Biochim. Biophys. Acta 388 (1975) 361–373.
[49] N. Yellin, I.W. Levin, Hydrocarbon chain disorder in lipid bilayers: temperature dependent Raman spectra of 1,2-diacylphosphatidylcholine–water gels, Biochim. Biophys. Acta 489 (1977) 177–190.
[50] N. Yellin, I.W. Levin, Hydrocarbon chain trans-gauche isomerization in phospholipid bilayer gel assemblies, Biochemistry 16 (1977) 642–647.
[51] C.B. Fox, R.H. Uibel, J.M. Harris, Detecting phase transitions in phosphatidylcholine vesicles by Raman microscopy and self-modeling curve resolution, J. Phys. Chem. B 111 (2007) 11428–11436.
[52] M. Rappolt, P. Laggner, G. Pabst, Structure and elasticity of phospholipid bilayers in the La phase: a comparison of phosphatidylcholine and phosphatidylethanolamine membranes, in: S.G. Pandalai (Ed.), Recent Research Developments in Biophysics, vol. 3, Transworld Research Network, Trivandrum, 2004, pp. 365–394, Part II.
[53] M.H.F. Wilkins, A.E. Blaurock, D.M. Engelman, Bilayer structure in membranes, Nat. New Biol. 230 (1971) 72–76.
[54] S. Tristram-Nagle, R. Zhang, R.M. Suter, C.R. Worthington, W.J. Sun, J.F. Nagle, Measurement of chain tilt angle in fully hydrated bilayers of gel phase lecithins, Biophys. J. 64 (1993) 1097–1109.
[55] M.J. Ruocco, G.G. Shipley, Characterization of the sub-transition of hydrated diplmitoyolphosphatidylcholine bilayers. Kinetic, hydration and structural study, Biochim. Biophys. Acta 691 (1982) 309–320.

[56] W.J. Sun, R.M. Suter, M.A. Knewtson, C.R. Worthington, S. Tristram-Nagle, R. Zhang, J.F. Nagle, Order and disorder in fully hydrated unoriented bilayers of gel phase dipalmitoylphosphatidylcholine, Phys. Rev. E 49 (1994) 4665–4676.
[57] W.J. Sun, S. Tristram-Nagle, R.M. Suter, J.F. Nagle, Structure of the ripple phase in lecithin bilayers, Proc. Natl. Acad. Sci. U. S. A. 93 (1996) 7008–7012.
[58] M. Rappolt, G. Rapp, Structure of the stable and metastable ripple phase of dipalmitoylphosphatidylcholine, Eur. Biophys. J. 24 (1996) 381–386.
[59] J.F. Nagle, S. Tristram-Nagle, Structure of lipid bilayers, Biochim. Biophys. Acta 1469 (2000) 159–195.
[60] J. Katsaras, S. Tristram-Nagle, Y. Liu, R.L. Headrick, E. Fontes, P.C. Mason, J.F. Nagle, Clarification of the ripple phase of lecithin bilayers using fully hydrated, aligned samples, Phys. Rev. E 61 (2000) 5668–5677.
[61] T.P. McMullen, R.N. McElhaney, New aspects of the interaction of cholesterol with dipalmitoylphosphatidylcholine bilayers as revealed by high-sensitivity differential scanning calorimetry, Biochim. Biophys. Acta 1234 (1995) 90–98.
[62] M. Rappolt, M.F. Vidal, M. Kriechbaum, M. Steinhart, H. Amenitsch, S. Bernstorff, P. Laggner, Structural, dynamic and mechanical properties of POPC at low cholesterol concentration studied in pressure/temperature space, Eur. Biophys. J. 31 (2003) 575–585.
[63] G. Pabst, H. Amenitsch, D.P. Kharakoz, P. Laggner, M. Rappolt, Structure and fluctuations of phosphatidylcholines in the vicinity of the main phase transition, Phys. Rev. E 70 (2004) 021908-1–021908-9.
[64] G. Pabst, J. Katsaras, V.A. Raghunathan, M. Rappolt, Structure and interactions in the anomalous swelling regime of phospholipid bilayers, Langmuir 19 (2003) 1716–1722.
[65] M. Rappolt, G. Rapp, Simultaneous small- and wide-angle X-ray diffraction during the main transition of dimyristoylphosphatidylethanolamine, Ber. Bunsenges. Phys. Chem. 100 (1996) 1153–1162.
[66] E. Theodoropoulou, D. Marsh, Interactions of angiotensin II non-peptide AT(1) antagonist losartan with phospholipid membranes studied by combined use of differential scanning calorimetry and electron spin resonance spectroscopy, Biochim. Biophys. Acta 1461 (1) (1999) 135–146.
[67] C. Fotakis, D. Christodouleas, P. Zoumpoulakis, A. Gili, E. Kritsi, N.P. Benetis, M. Zervou, H. Reis, M. Papadopoulos, T. Mavromoustakos, Comparative biophysical studies of sartan class drug molecules losartan and candesartan (CV-11974) with membrane bilayers, J. Chem. Phys. B 115 (19) (2011) 6180–6192.
[68] C. Fotakis, S. Gega, E. Siapi, C. Potamitis, K. Viras, P. Moutevelis-Minakakis, G. Kokotos, S. Durdagi, S. Grdadolnik, B. Sartori, M. Rappolt, T. Mavromoustakos, Drug interactions at the bilayer interface and receptor site induced by the novel synthetic pyrrolidinone analog MMK3, Biochim. Biophys. Acta 1798 (3) (2010) 422–432.
[69] X. Tian, S. Pavlopoulos, Y. De-Ping, A. Makriyannis, The interaction of cannabinoid receptor agonists, CP55940 and WIN55212–2 with membranes using solid state ^{2}H NMR, Biochim. Biophys. Acta 1808 (9) (2011) 2095–2101.
[70] I. Tadeusz, A. Gumieniczek, A. Kasinska, Chromatographic evaluation of lipophilicity for angiotensin II AT1 receptor antagonists, Annales Universitatis Marie Curie-Sklodowska Lublin-Polonia, 21(1), 2008, pp. 23–29.
[71] T. Mavromoustakos, E. Theodoropoulou, De-Ping Yang, The use of high resolution solid-state NMR spectroscopy and differential scanning calorimetry to study interactions of anaesthetic steroids with membrane, Biochim. Biophys. Acta 1328 (1997) 65–73.
[72] T. Mavromoustakos, De-Ping Yang, A. Makriyannis, Effects of the anaesthetic steroid alphaxalone and its inactive Δ^{16}-analog on the thermotropic properties of membrane bilayers. A model for membrane perturbation, Biochim. Biophys. Acta 1239 (1995) 257–264.
[73] J.S. Santos, D.K. Lee, A. Ramamoorthy, Effects of antidepressants on the conformation of phospholipid headgroups studied by solid-state NMR, Magn. Reson. Chem. 42 (2004) 105–114.
[74] T.J. O'Leary, P.D. Ross, I.W. Levin, Effects of anesthetic and non anesthetic steroids on dipalmitoylphosphatidylcholine liposomes: a calorimetric and Raman spectroscopic investigation, Biochemistry 23 (1984) 4636–4641.
[75] C. Potamitis, P. Chatzigeorgiou, E. Siapi, T. Mavromoustakos, A. Hodzic, F. Cacho-Nerin, P. Laggner, M. Rappolt, Interactions of the AT1 antagonist valsartan with dipalmitoyl-phosphatidylcholine bilayers, Biochim. Biophys. Acta 1808 (2011) 1753–1763.
[76] N.B. Colthulp, L.H. Daly, S.E. Wiberley, Introduction to Infrared and Raman Spectroscopy, Academic Press, 1990.
[77] I.W. Levin, R.N. Lewis, Fourier transform Raman spectroscopy of biological materials, Anal. Chem. 62 (1990) 1101A–1111A.
[78] R.K. Bista, R.F. Bruch, A.M. Covington, Variable-temperature Raman spectromicroscopy for a comprehensive analysis of the conformational order in PEGylated lipids, J. Raman Spectrosc. 40 (2008) 463–471.
[79] B.P. Gaber, W.L. Peticolas, On the quantitative interpretation of biomembrane structure by Raman spectroscopy, Biochim. Biophys. Acta 465 (1977) 260–274.
[80] C. Fotakis, D. Christodouleas, P. Chatzigeorgiou, M. Zervou, N.P. Benetis, K. Viras, T.M. Mavromoustakos, Application of a novel CP-^{31}P NMR methodology to study the possible interdigitation effect of losartan in phospholipids bilayers. Comparison with Raman spectroscopy data, Biophys. J. 96 (2009) 2227–2236.
[81] N.P. Benetis, I. Kyrikou, T. Mavromoustakos, M. Zervou, Static ^{31}P CP NMR multilamellar bilayer broadlines in the absence and presence of the bioactive dipeptide beta-Ala-Tyr or Glu, Chem. Phys. 314 (1–3) (2005) 57–72.
[82] I. Kyrikou, S. Xadjikakou, D. Kovala-Demertzi, K. Viras, T. Mavromoustakos, Effects of non steroid anti-inflammatory drugs in membrane bilayers containing cholesterol, Chem. Phys. Lipids 132 (2004) 157–169.
[83] E. Bicknell-Brown, K.G. Brown, Raman temperature study of conformational changes in anhydrous dipalmitoylphosphatidylcholine, Biochim. Biophys. Acta 778 (1984) 317–323.
[84] A.L. Jenkins, R.A. Larsen, T.B. Williams, Characterization of amino acids using Raman spectroscopy, Spectrochim. Acta A 61 (2005) 1585–1594.
[85] R. Nakagomi-Hagihara, D. Nakai, K. Kawai, Y. Yoshigae, T. Tokui, T. Abe, T. Ikeda, OATP1B1, OATP1B3, and MRP2 are involved in hepatobiliary transport of olmesartan, a novel angiotensin II blocker, Drug Metab. Dispos. 34 (2006) 862–869.
[86] E. Cagigal, L. Gonzalez, R.M. Alonso, R.M. Jimenez, pKa determininationof angiotensin II receptor antagonists (ARA II) by spectrofluorimetry, J. Pharm. Biomed. Anal. 26 (2001) 477–486.
[87] T. Kikuchi, N. Ito, M. Suzuki, A. Kusai, K. Iseki, H. Sasaki, Self-association properties of 4-[1-hdyroxy-1-methylethyl]-2-propyl-1-[4-[tetrazole-5yl]phenyl]phenyl] methylimidazole-5-carboxylic acid monohydrate (CS-0880, an antiglaucoma ophthalmic agent, Int. J. Pharm. 299 (2005) 100–106.